



RESEARCH

A micromagnetic study of sample size effects on dynamic hysteresis properties and dynamic phase transitions of Fe and Fe_3O_4 nanodisks

Necda Çam

Received: 9 July 2024 / Accepted: 4 September 2024
© The Author(s), under exclusive licence to Springer Nature B.V. 2024

Abstract The influence of size on the dynamic magnetic hysteresis properties and dynamic phase transitions of Fe and Fe_3O_4 2D-circular nanodisks with varying diameters has been explored in the micromagnetic framework. This investigation is conducted under a sinusoidal dynamic magnetic field along the x-direction by solving the Landau-Lifshitz-Gilbert (LLG) equation with the OOMMF software at zero temperature. The dynamic hysteresis of nanodisks is profoundly impacted by both the frequency and amplitude of the applied external field, along with the particle size. As particle size decreases, there is an observed increase in the frequency values at which the transition to dynamic ordered frequency occurs in Fe nanodisks, whereas a decrease is noted in the transition frequency values of Fe_3O_4 nanodisks.

Keywords Dynamic hysteresis · Fe nanodisks · Fe_3O_4 nanodisks · Micromagnetism · LLG equation · Hysteresis loop area; coercive field · Remanent magnetization · Model and simulation

Research Highlights:

- The dynamic phase transitions in Fe_3O_4 and Fe nanodisks with varying diameters are explored.
- Time series and hysteresis loops have been calculated within the micromagnetic framework.
- HLA, RM, and CF values from the dynamic hysteresis characteristics have been obtained as functions of frequency.

1 Introduction

Magnetic nanoparticles, with their non-linear optical, magnetic, and electronic properties, have recently garnered significant attention from researchers across various advanced areas such as high-density digital storage [1], magnetic sensors [2], hyperthermia therapy [3], drug delivery [4], environmental [5], and industrial applications [6] both from a fundamental and technological perspective.

Nanoparticles are distinguished distinctly from other magnetic materials, primarily due to their finite size and high aspect ratio effects [7]. As the size of the nanoparticle decreases, most of the spins are located on the surface [8]. Therefore, changes in some local physical properties of the nanostructured material, such as a decrease in exchange interaction constants and saturation magnetization or an increase in local

N. Çam (✉)
Department of Physics, Dokuz Eylül University, TR-35160
Izmir, Turkey
e-mail: necda.cam@ogr.deu.edu.tr

anisotropy, may stem from a disordered spin pattern on the nanoparticle surface [9]. Through deliberate shape- and surface-controlled synthesis, these aspects can be more precisely modulated, offering a more controllable approach to magnetic properties [10].

Furthermore, the adjustment of coercivity and magnetization through the size and shape of nanostructures is key to enhancing performance in technological applications [11], whereas hyperthermia treatment necessitates biocompatibility and high specific absorption rate (SAR) values where magnetic energy is absorbed and transformed into thermal energy as crucial factors [12]. Due to their non-toxic nature, iron oxide nanoparticles (Fe_3O_4) emerge as excellent candidates for magnetic hyperthermia under alternating magnetic fields [13]. Thus, various magnetic properties of Fe_3O_4 nanoparticles with varying sizes and shapes have been extensively discussed in numerous studies in the literature [14]–[17]. For example, the effect of surface and size on coercivity in M-type hexagonal ferrites has been addressed by Haseeb et al. via both experimentally and micromagnetic modeling [18]. They have found that larger particle sizes and the presence of surface defects contribute to a decrease in coercivity. Jalali et al. have examined the influence of various shapes of Fe_3O_4 nanoparticles on the loss tangent and magnetic permeability values under a dynamic magnetic field with frequencies ranging from 0.5 to 20 GHz [19]. Their findings indicated that elongated nanoparticles displayed elevated microwave magnetic permeability values, whereas the impact of elongation on resonance frequencies varied among spherical and prismatic nanoparticles. Tsuji and Kobayashi have conducted micromagnetic studies on hollow nanoparticles ranging in size between 696 and 100 nm [20]. They determined that hollow nanostructures with an inner/outer diameter ratio of 0.5 and a size of 296 nm have exhibited the highest SAR, which is comparable to traditional superparamagnets. The examination of tunnel magnetoresistance [21], resonance modes [22], and the responses of easy-axis orientation in dynamic magnetic field [23] have also been reported for Fe_3O_4 recently.

From a technological standpoint, perhaps one of the most captivating nanoparticles are those composed of iron (Fe) [24]. The balanced interplay between magneto-crystalline and shape anisotropies in Fe frequently facilitates the emergence of intriguing mag-

netic states and magnetization reversal mechanisms [25]. Leighton et al. have investigated the coercivity and remanent magnetization of asymmetric Fe nanodisks with different sizes and thicknesses subjected to a static field [26]. They have emphasized that asymmetry significantly alters the magnetic behavior, and changing the angle of the applied magnetic field induces the reversal process response from vortex mode to coherent mode. The dynamic susceptibility spectra of square [27] and spherical [28] nanostructures with different aspect ratios have been calculated by the same group under a weak dynamic field. They have revealed that the main source of resonance mode in square nanostructures is due to dipolar interaction. Furthermore, the magnetic properties of Fe nanoparticles with different shapes, such as asymmetric rings [29], superellipses [30], hexagonal [31], nanomagnets with Reuleaux's triangle, circle, and triangle geometry [32], have been investigated.

According to the literature mentioned above, the interesting magnetic behavior of Fe_3O_4 and Fe nanodisks has attracted great attention from researchers. However, the effect of diameter on the dynamic hysteresis characteristics and the dynamic phase transition behavior of nanodisks has not been discussed yet. This size is particularly crucial due to the relationship between the frequency of the applied sinusoidal external magnetic field and the relaxation time of the system. The system can follow the magnetic field called the dynamically disordered phase or cannot follow the magnetic field called the dynamically ordered phase. The correlation between dynamic phase transitions and the magnetic behavior resulting from a decreasing diameter requires comprehensive investigation, both from a fundamental scientific perspective and in terms of potential applications. Therefore, the aim of this study is to investigate the dynamic magnetic properties of Fe and Fe_3O_4 nanodisks subjected to dynamic magnetic field, in order to gain insights into both their potential technological applications and phase transitions. To exclude thermal fluctuations, simulations have been performed at zero temperature, we have only focused on investigating the combined effects of system size, exchange interactions, dipolar interactions, anisotropy energy, and Zeeman energy on the dynamic phase transitions and dynamic hysteresis characteristics of Fe and Fe_3O_4 nanodisks subjected to a time-dependent sinusoidal magnetic field.

The paper is organized as follows: In Sec. 2, we briefly present the model and formulation. The results and discussions are presented in Sec. 3, and finally, Sec. 4 contains our conclusions.

2 Model and formulation

Figure 1 depicts the flat, circular, two-dimensional *Fe* and *Fe₃O₄* nanodisks with diameters of $D = 270\text{ nm}$, $D = 120\text{ nm}$, and $D = 90\text{ nm}$, respectively, oriented in the *xy*-plane, as addressed in this study.

Landau-Lifshitz-Gilbert (LLG) equation that governs the system’s magnetization dynamics is presented below:

$$\frac{d\mathbf{m}}{dt} = -\gamma \mathbf{m} \times \mathbf{H}_{\text{eff}} - \alpha \mathbf{m} \times (\mathbf{m} \times \mathbf{H}_{\text{eff}}) \tag{1}$$

where $\mathbf{m} = \mathbf{M}/M_s$ denotes the normalized magnetization, signifying the magnetization of the system scaled by the saturation magnetization M_s . α and γ used in numerical calculations are the damping coefficient and the gyromagnetic ratio, respectively. \mathbf{H}_{eff} denotes the effective field. The effective field is determined by differentiating the total energy with respect to magnetization:

$$\mathbf{H}_{\text{eff}} = -\frac{1}{\mu_0} \frac{\partial E}{\partial \mathbf{m}}, \tag{2}$$

where E is the total energy and includes the contribution of four main energy terms: exchange, anisotropy, demagnetization, and Zeeman energy terms. The con-

tinuum form of these energies in micromagnetics can be expressed by the following equations, respectively:

$$E_{\text{ex}} = \int d^3r \frac{A}{M_s^2} (|\nabla m_x|^2 + |\nabla m_y|^2 + |\nabla m_z|^2), \tag{3}$$

$$E_{\text{an}} = \int d^3r \frac{K}{M_s^2} (\mathbf{m} \cdot \mathbf{u})^2, \tag{4}$$

$$E_{\text{demag}} = \frac{\mu_0}{8\pi} \int d^3r \mathbf{m}(\mathbf{r}) \cdot \left[\int d^3r' \nabla \cdot \mathbf{m}(\mathbf{r}') \frac{\mathbf{r} - \mathbf{r}'}{|\mathbf{r} - \mathbf{r}'|^3} - \int d^2r' \hat{\mathbf{n}} \cdot \mathbf{m}(\mathbf{r}') \frac{\mathbf{r} - \mathbf{r}'}{|\mathbf{r} - \mathbf{r}'|^3} \right], \tag{5}$$

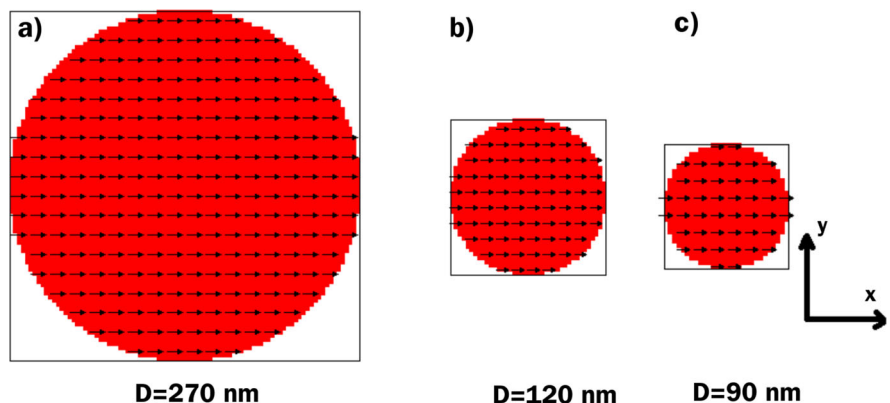
$$E_{\text{Zeeman}} = -\mu_0 \int d^3r \mathbf{m} \cdot \mathbf{H}_{\text{ext}}. \tag{6}$$

Here, A is the exchange stiffness constant, K is the anisotropy constant, \mathbf{u} is the anisotropy direction, μ_0 is the permeability of free space, and \mathbf{H}_{ext} is the external magnetic field. By solving the nonlinear LLG equation given in Eq. 1, one can obtain the time evolution of the magnetization components, $m_\alpha(t)$ ($\alpha = x, y, z$) associated with the system. The integral is utilized to compute the dynamic order parameter of the system:

$$Q_\alpha = \frac{1}{P} \int_T^{T+P} m_\alpha(t) dt, \quad \alpha = x, y, z \tag{7}$$

The integral is computed over one period (P) of the system, where T represents an arbitrary time. This lower limit of integration is essential for excluding the transient region of the magnetization’s time series.

Fig. 1 Visualization of the nanodisks size with varying diameter D for *Fe* and *Fe₃O₄* nanodisks at +*x*-aligned initial magnetic spin configuration



The dynamic order parameter determines the dynamic order of the system. A value of $Q = 0$ corresponds to the dynamically disordered phase, whereas a non-zero value of the dynamical order parameter signifies the dynamically ordered phase. The relationship between the relaxation time of the system and the period of time-varying external magnetic field dictates the dynamical phase of the system. When the magnetization of the system can track a time-dependent magnetic field, it indicates that the system is in a dynamically disordered phase (or, in other words, it is referred to as the dynamic paramagnetic phase) where Q is zero. Conversely, a nonzero dynamical order parameter suggests that the magnetization cannot precisely follow the driving field where the system is in the dynamically ordered phase (or, in other words, it is referred to as the dynamic ferromagnetic phase).

The main factor contributing to the dynamical hysteresis behavior is a delay in the magnetization process in response to the applied magnetic field. The hysteresis loop of the system reflects the variation of the magnetization component with the external magnetic field over one period of the field. The quantities that describe the characteristics of dynamic hysteresis loops include the hysteresis loop area (HLA), remanent magnetization (RM), and coercive field (CF). The HLA also refers to the region enclosed by the hysteresis loop, which arises from the interaction between magnetization and the magnetic field. HLA relates to heat dissipation in the system. While the RM represents the remaining magnetization after the removal of the external magnetic field in the system, the CF corresponds to the field amplitude required to reverse the magnetization's direction in the system. CF also provides additional information on the hysteresis curve's width. In equilibrium systems, the coercive field value is observed within the ferromagnetic phase, whereas in nonequilibrium systems subjected to a dynamic magnetic field, it manifests only within the dynamical paramagnetic phase.

The transition from the dynamic disordered phase to the dynamic ordered phase is determined as follows:

hysteresis loops are calculated separately for each frequency over a duration of 20 ns and then averaged to produce a single hysteresis cycle. The HLA, RM, and CF values of the averaged hysteresis loop for each frequency are calculated individually. In the dynamic disordered phase, RM values exhibit both negative and positive values in two branches, whereas in the dynamic ordered phase, RM values are positive in only two branches. Additionally, CF values in the dynamic ordered phase are zero, as the CF curve does not intersect the x-axis. In contrast, the CF curve in the dynamic disordered phase intersects the axis at both negative and positive values. The frequencies at which RM values appear in the positive branch and CF values are zero are identified as the phase transition frequencies. After comparing RM and CF values individually, they are also evaluated against the Q_α parameter, which represents the average of the magnetization components at each frequency. The integral used to calculate the Q_α parameter is given in Eq. 7. The transition frequency to the dynamically ordered phase is pinpointed by the frequency at which the Q_α parameter becomes nonzero. Thus, the transition frequency is determined by a meticulous comparison of RM, CF, and Q_α values.

To solve the LLG equation, we have utilized the OOMMF software based on finite difference numerical approximation [33]. The damping coefficient α in Eq. 1 is set at 0.01 and 0.025 for Fe and Fe₃O₄, respectively, which is typical for the dynamical solution of the LLG equation [34]. The cell size of the nanodisks (which is necessary for the discretization of the geometry of the system) is chosen as 3 nm, which is consistent with the exchange length defined by $l_{ex} \approx \sqrt{2A / (\mu_0 M_s^2)}$ [35]. Dynamic hysteresis has been obtained within a total simulation duration of 20 ns, following an assessment of its suitability to capture the phase transition dynamics of the system. Each of the hysteresis characteristics has been computed by averaging the hysteresis obtained during this duration. The required parameters for Fe and Fe₃O₄ utilized in numerical calculations are presented in Table 1 [31], [36]. In accordance with

Table 1 Material-specific parameter values for the calculation

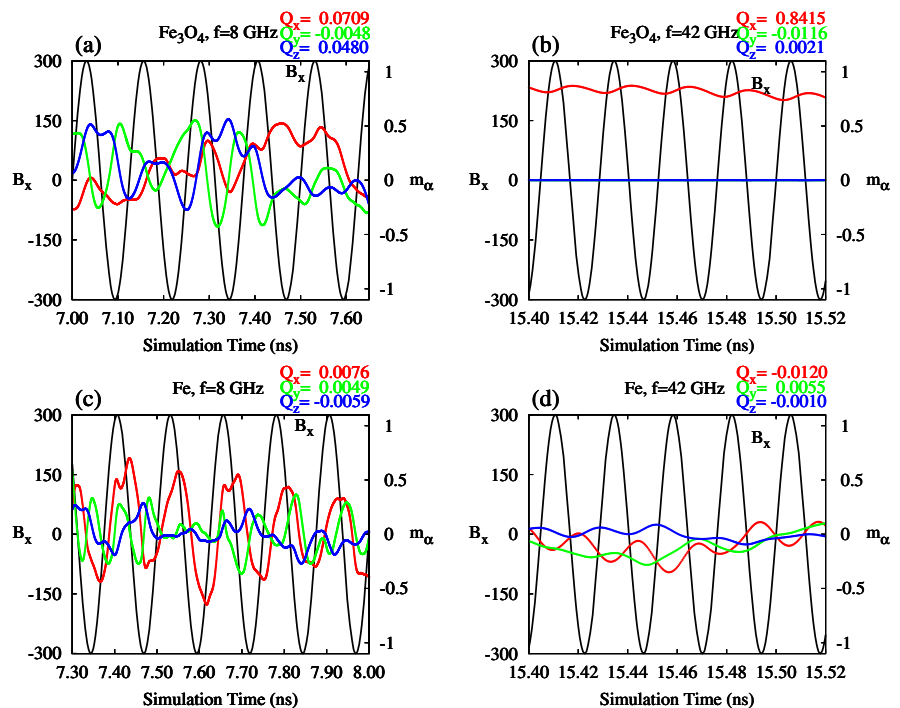
Materials	M_s [A/m]	A [J/m]	K [J/m ³]	l_{ex} nm
Iron (Fe)	1700×10^3	21×10^{-12}	48×10^3 (cubic)	3.4
Magnetite (Fe ₃ O ₄)	480×10^3	15.3×10^{-12}	-	10.2

the literature, the magnetocrystalline anisotropy axes for Fe have been selected as easy cubic, with orientations at 0° and 90° . Fe_3O_4 is considered a soft magnetic material; the anisotropy constant K is neglected, as indicated in ref [36].

3 Results and discussion

This study has examined Fe and Fe_3O_4 nanodisks with diameters varying at 90 nm , 120 nm , and 270 nm . The nanodisks have been assumed to be flat, circular, and situated in the two-dimensional xy -plane. When the cell size and nanodisks thickness are the same, systems have been configured as a two-dimensional system in the OOMMF software. Therefore, 900, 1600, and 8100 cells correspond to 2D-nanodisks with 90 nm , 120 nm , and 270 nm , respectively. Before starting the simulation, the initial spin configurations are selected to be aligned along the $+x$ -direction for all nanostructures, as depicted in Fig. 1. Simulations were also performed with various coordinates (x, y, z) along with random orientations, and the final magnetic results remained unchanged. Because the final dynamic magnetic responses are identical, we prefer the x -aligned spin configuration for our initial spin configuration.

Fig. 2 A typical low- and high-frequency time series of Fe_3O_4 (a, b) and Fe (c, d) nanodisks with 120 nm diameter for $B_0 = 300\text{ mT}$



The magnetic field is considered to be in the x -direction and can be expressed as follows:

$$B_x = B_0 \sin \omega t, \tag{8}$$

where t is the time and $\omega = 2\pi f$, f is the frequency in units of GHz . The amplitudes of the field chosen are $B_0 = 100\text{ mT}$ and 300 mT . In order to capture phase transitions, the frequency range is selected between $1 - 50\text{ GHz}$ for Fe_3O_4 , while $1 - 60\text{ GHz}$ is set for Fe . To exclude the effects of thermal fluctuations, simulations have been carried out at zero temperature. The focus of these simulations is on analyzing the interplay between system size, exchange interactions, dipolar interactions, anisotropy energy, and Zeeman energy with respect to dynamic phase transitions and dynamic hysteresis phenomena in Fe and Fe_3O_4 nanodisks under the influence of a time-dependent sinusoidal magnetic field.

3.1 Behavior of the dynamical hysteresis

Figure 2 shows the time series for Fe and Fe_3O_4 nanodisks with 120 nm diameter under a 300 mT magnetic field at both high and low frequencies. The corresponding dynamic order parameter values (Q_x, Q_y, Q_z ,

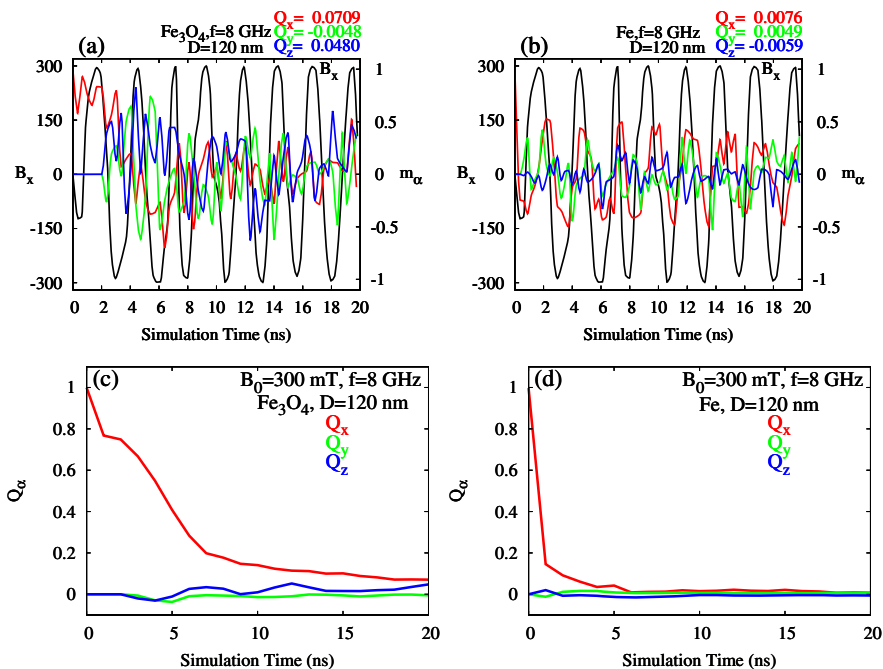
Q_z) at low- and high-frequency values are also given. In Fig. 2a and c, it is seen that the magnetization components follow the field with a delay at $f = 8 \text{ GHz}$. This delay is the source of dynamic hysteresis behavior. When the frequency value reaches 42 GHz in Fig. 2d, the Fe nanodisks can still follow the external dynamic magnetic field with a delay ($Q_\alpha = 0$) which corresponds to the dynamic disordered phase. However, the x magnetization component of the Fe_3O_4 nanodisks cannot follow the field ($Q_x \neq 0$) in Fig. 2b. In other words, Fe_3O_4 nanodisks transitioned into a dynamically ordered phase with an increasing frequency value. Nanodisks with the same diameter have completely different dynamic order parameters at high frequency, which causes their dynamic hysteresis behavior to differ and will be examined in detail.

To obtain more detailed information about the general behavior of the time series, the typical behavior of the magnetization components of 120 nm Fe and Fe_3O_4 nanodisks under a 300 mT magnetic field over the entire simulation duration 20 ns is shown in Fig. 3. To simplify the extensive data on the magnetic field and magnetization components collected over the 20 ns period, values were sampled every 1000 steps. This summarized data is shown in Fig. 3a and b. As depicted, the x component of the magnetization at 0 ns is +1, reflecting the initial spin configuration aligned

along the +x direction in both systems, while the other two components remain at zero. As the sinusoidal field varies over time, the magnetization components respond accordingly, though with a delayed reaction. The key difference observed in the graph between the Fe and Fe_3O_4 nanosystems is that the magnetization components in the Fe_3O_4 system align with the magnetic field only after about 3 ns , while Fe exhibits a quicker response. Consequently, the initial magnetic behaviors during this period were excluded from the hysteresis averaging. Once the system's response stabilized against the dynamic magnetic field, the average hysteresis loop was computed. Additionally, Fig. 3c and d show the characteristic changes in Q_α over 20 ns for Fe and Fe_3O_4 nanodisks.

Figure 4 presents hysteresis loops that illustrate the dynamic reversal process for Fe_3O_4 nanodisks with 90 nm and 270 nm diameters at different frequencies. At low frequency in Fig. 4a, all three components of the magnetization of Fe_3O_4 nanodisks with a diameter of 90 nm respond by following the time-dependent magnetic field, resulting in dynamically disordered phase hysteresis loops. When the frequency value is 16 GHz , m_x and m_y hysteresis continue to follow the magnetic field with narrowing hysteresis loops, while the m_z magnetization component cannot follow the dynamic field and shows weak dynamic order and nar-

Fig. 3 A time series and Q_α variations of Fe_3O_4 and Fe nanodisks with 120 nm diameter at $B_0 = 300 \text{ mT}$ with $f = 8 \text{ GHz}$ for simulation duration 20 ns



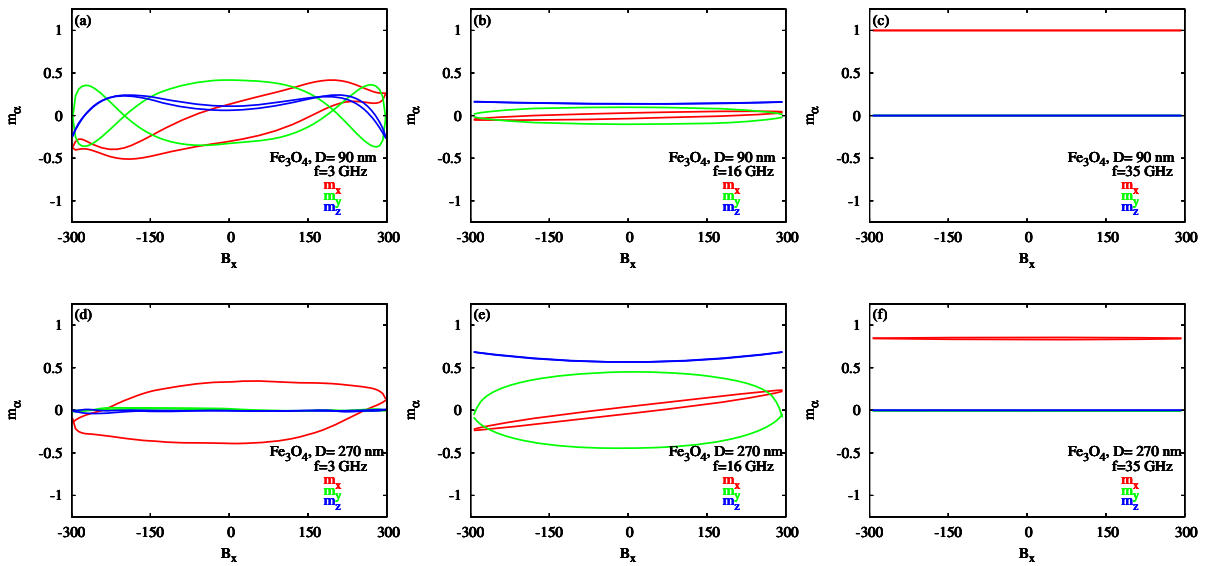


Fig. 4 Variation of the hysteresis loops of Fe_3O_4 nanodisks according to different frequencies and diameter values at $B_0 = 300\text{ mT}$

row dynamic ordered phase hysteresis loop in Fig. 4b. As the frequency increases further to 35 GHz in Fig. 4c, the m_x magnetization component of the Fe_3O_4 system cannot follow the time-dependent field this time, and the system exhibits typical high dynamically ordered hysteresis loop behavior.

As the diameter of the nanodisks increases (in 270 nm), different dynamic hysteresis processes are

observed at each frequency value. In Fig. 4d, only the m_x magnetization component follows the magnetic field at low frequencies, whereas the m_y and m_z components do not display hysteresis behavior, as opposed to the system with 90 nm diameter. For $f = 16\text{ GHz}$ in Fig. 4e, it can be seen that the hysteresis loop produced by m_x is still in the dynamically disordered phase. On the other hand, the m_y magnetization component pro-

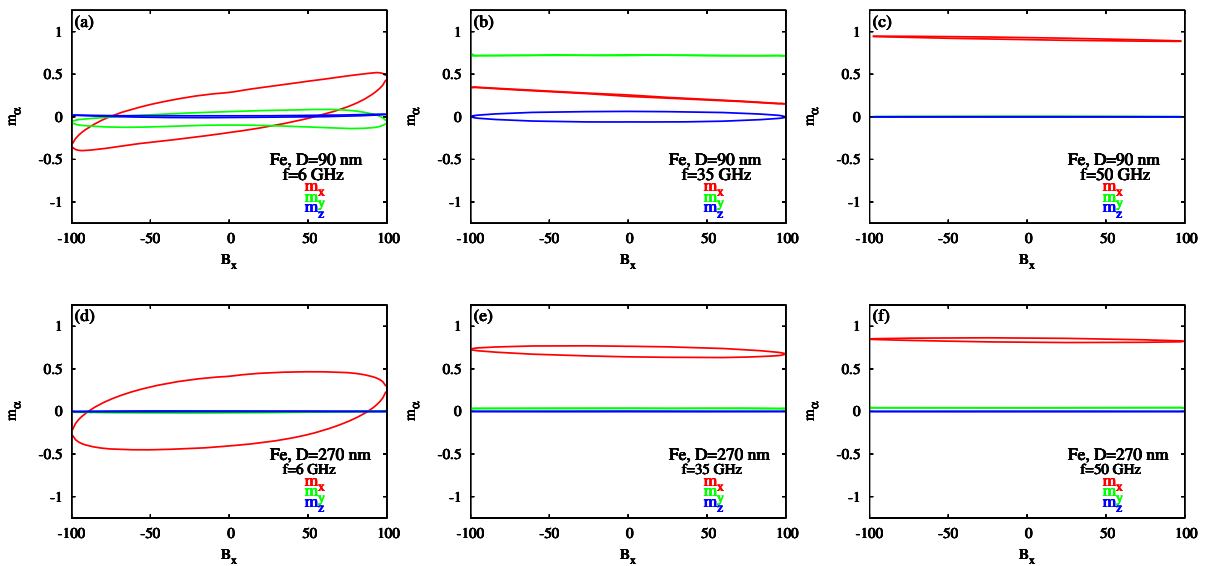


Fig. 5 Variation of the hysteresis loops of Fe nanodisks according to different frequencies and diameter values at $B_0 = 100\text{ mT}$

duces dynamic disordered hysteresis despite the application of a magnetic field in the x -direction and is even wider than the hysteresis loop created by m_x . Moreover, it is seen that the m_z magnetization component is in a higher dynamic order compared to the Fe_3O_4 system with a diameter of 90 nm at the same frequency value. In the system with a diameter of 270 nm , a similar dynamic reversal process has been observed at a high frequency in Fig. 4f as 90 nm , but a relatively lower dynamic order was observed. The hysteresis loops at the chosen frequency values are evidently impacted by the size, which also has a significant impact on determining the dynamic phase behavior.

To examine the variations in the dynamic hysteresis of Fe nanodisks with diameters of 90 nm and 270 nm at varying frequency values under a constant dynamic magnetic field $B_0 = 100\text{ mT}$, Fig. 5 has been plotted. At low frequency, Fe and Fe_3O_4 systems appear to have similar hysteresis loop processes. At $f = 35\text{ GHz}$, as depicted in Fig. 5b, the magnetization components m_x and m_y exhibit an inability to track the field, leading to the manifestation of dynamically ordered phase hysteresis within the x -directed dynamic magnetic field. Conversely, the m_z component displays a response to the field characterized by dynamic disordered phase hysteresis. Figure 5e clearly illustrates that increasing diameter results in the suppression of the behaviors exhibited by the m_y and m_z components.

Consequently, diameter enhancement allows the m_x magnetization component to generate increased levels of dynamic phase hysteresis. When the frequency reaches 50 GHz , 90 nm and 270 nm have similar hysteresis loop processes, but the increase in diameter supports the expansion of the hysteresis loop in big nanodisk. As the diameter increases (270 nm), more magnetic moments are present, leading to strengthened interactions within the system. This diminishes the system's tendency to align with the external magnetic field, contributing to the weaker dynamic order hysteresis observed compared to 90 nm diameter nanostructures.

3.2 Characteristics of the dynamical hysteresis

To get more detailed information about dynamic hysteresis characteristics, HLA, RM, and CF values have been comprehensively calculated from the hysteresis curves obtained via micromagnetic simulations. We set the magnetic field to $B_0 = 100\text{ mT}$ and $B_0 = 300\text{ mT}$, while to capture phase transitions, we set the frequency range as $f = 1 - 50\text{ GHz}$ for Fe_3O_4 nanodisks and $f = 1 - 60\text{ GHz}$ for Fe nanodisks.

Firstly, the change of HLA for Fe_3O_4 nanodisks according to frequency and diameter is presented in Fig. 6. As depicted in Fig. 6a, for the nanostructure with a diameter of 90 nm , the HLA curve repre-

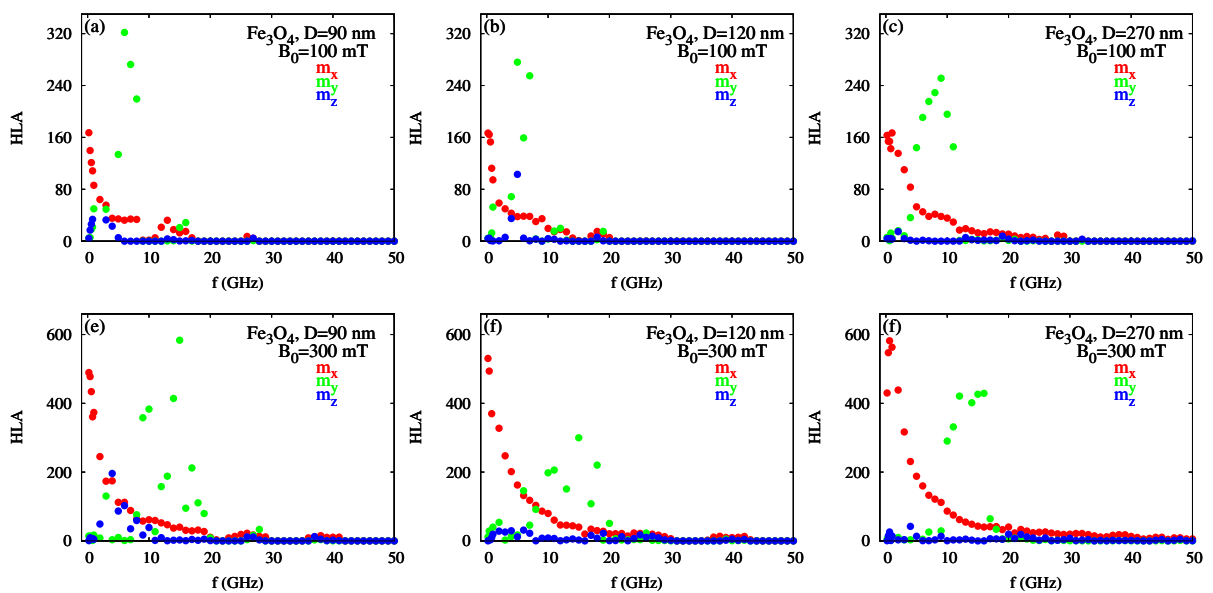


Fig. 6 Dependence of HLA values of Fe_3O_4 nanodisks on changing diameter and frequency for $B_0 = 100\text{ mT}$ $B_0 = 300\text{ mT}$

sented by the m_x magnetization component decreases as the frequency increases from its peak value. After $f = 10\text{ GHz}$, it reached a second small peak value and decreased again. The absence of a trend indicates that there are some frustrations in the system due to small size effects. Interestingly, in the system with a big diameter and a sinusoidal field applied in the x -direction, the highest hysteresis loop area values are produced by the m_y component, which reaches its maximum value around $f = 6\text{ GHz}$. The m_z component also has the lowest HLA values in the nanodisks system and disappears after around 3 GHz . In Fig. 6d, HLA values generally increased when the amplitude is $B_0 = 300\text{ mT}$. In the HLA curve produced by m_y , variations emerge with increasing frequencies without displaying a clear increasing or decreasing trend. The reason for this situation can be attributed to reducing the diameter of the system and the exposure to a high magnetic field. Because when the diameter increases to $120\text{--}270\text{ nm}$, this situation begins to disappear. Similar HLA trends are seen in the system with a diameter of 120 nm in Fig. 6b and e. However, the HLA peak formed by m_y values is reduced. On the other hand, increasing the diameter generally led to the formation of HLA curves exhibiting a more regular trend which can be seen in Fig. 6c and f. In particular, in Fig. 6f, at the amplitude value of 300 mT , HLA produced by m_x started from its minimum value and then reached its

peak value, in opposition to the other five plots. With increasing magnetic dipole moments and increasing D parameter in the 270 nm system, the m_x value representing HLA at 300 mT starts at its minimum, peaks, and then declines, in contrast to other curves as shown in Fig. 6f.

Figure 7 shows the variation in HLA for the Fe nanodisk with respect to frequency and diameter at various amplitude values. At all diameter values, Fe nanodisks typically exhibit greater HLA values than Fe_3O_4 nanodisks, with HLA declining towards high-frequency values. The HLA curves formed by the m_y and m_z magnetization components in the Fe are limited to a narrower frequency range. For 90 nm diameter nanodisks, only in the 100 mT m_y -HLA and m_z -HLA curve (m_y for approximately $1\text{--}10\text{ GHz}$, m_z for approximately $33\text{--}39\text{ GHz}$) and in 300 mT , m_y -HLA curves are observed in Fig. 7a and d. For 120 nm diameter nanodisks, only in the 100 mT , m_y -HLA curve (m_y for approximately $1\text{--}13\text{ GHz}$, m_z for approximately $35\text{--}44\text{ GHz}$) is seen in Fig. 7b. m_y and m_z behavior is diminished through enhanced amplitude and diameter. As the diameter increases at an amplitude of 100 mT , the maximum of the m_x HLA curve decreases. Conversely, at 300 mT , it exhibits an increase.

The magnetocrystalline anisotropy, strong exchange interaction, and high saturation value of Fe nanodisks

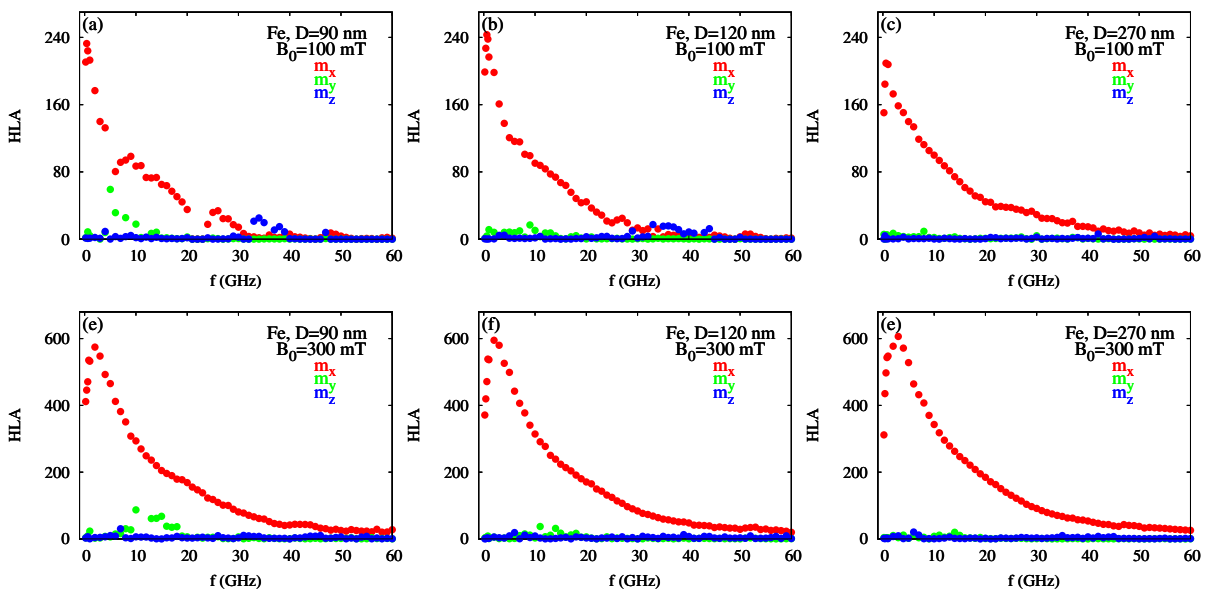


Fig. 7 Dependence of HLA values of Fe nanodisks on changing diameter and frequency for $B_0 = 100\text{ mT}$ $B_0 = 300\text{ mT}$

alleviate the frustrated effects induced by particle size reduction in the system. This ensured that the magnetic moments remained in-plane. Consequently, this facilitates the formation of more stable HLA and RM curves compared to Fe_3O_4 .

The second hysteresis characteristic under consideration is RM, namely remanence magnetization. RM provides valuable insights into dynamic phase transitions. The RM values of Fe_3O_4 nanodisks are depicted in Fig. 8. In all graphs, the m_x -RM exhibits two arms, positive and negative, indicating the dynamic disordered phase at the initial frequency values. As the frequency increased, the two-arm behavior decreased to a single arm after about 9 GHz in Fig. 8a and b, suggesting the system transitioned into the dynamic ordered phase. At the same time, interestingly, in the system around 5–8 GHz, while m_z is in the dynamically ordered phase, m_y is in the dynamically disordered phase. This situation occurs before m_x transitions to the dynamic ordered phase. As observed in Fig. 8d and e, increasing the amplitude value led to a difference in the dynamic phase transition frequency value for the two diameters. The frequency range associated with dynamic ordered phase, represented by the m_z magnetization component, and with dynamic disordered phase behavior, represented by the m_y magnetization component, has shifted to higher frequencies. On the other hand, increasing the diameter supported the prominent

increasing and decreasing trend in the curves and the clear observation of the dynamic phase transition frequency. It is evident from Fig. 8c that at high-frequency values, the RM values of m_x tend to be at 1. However, RM values decrease when the amplitude is 300 mT in Fig. 8d.

Figure 9 is illustrated to provide detailed insights into the frequency-dependent behavior of Fe nanodisks with different diameters. A distinctly different behavior is observed compared to Fe_3O_4 nanodisks. As depicted in Fig. 9a–c, at low amplitude, there is a notable shift towards lower frequencies in the transition frequency values from the dynamic disordered phase to the dynamic ordered phase as the diameter increases for the m_x -remanence magnetization. This observation contrasts with the behavior observed in Fe_3O_4 nanodisks. Additionally, while around 33–39 GHz, the RM associated with the m_y distinctly reveals the presence of dynamic ordering along this axis, the RM associated with the m_z magnetization component resides within the dynamic disordered phase. At high frequencies, it can also be observed that the RM values decrease as the diameter increases (by comparing Fig. 9a and c). When the amplitude increases in Fig. 9d–f, the dynamic phase transition frequency values for systems with diameters of 90 nm and 120 nm are approximately 58 GHz and 54 GHz, respectively. However, when the diameter is sufficiently large, 270 nm, the system

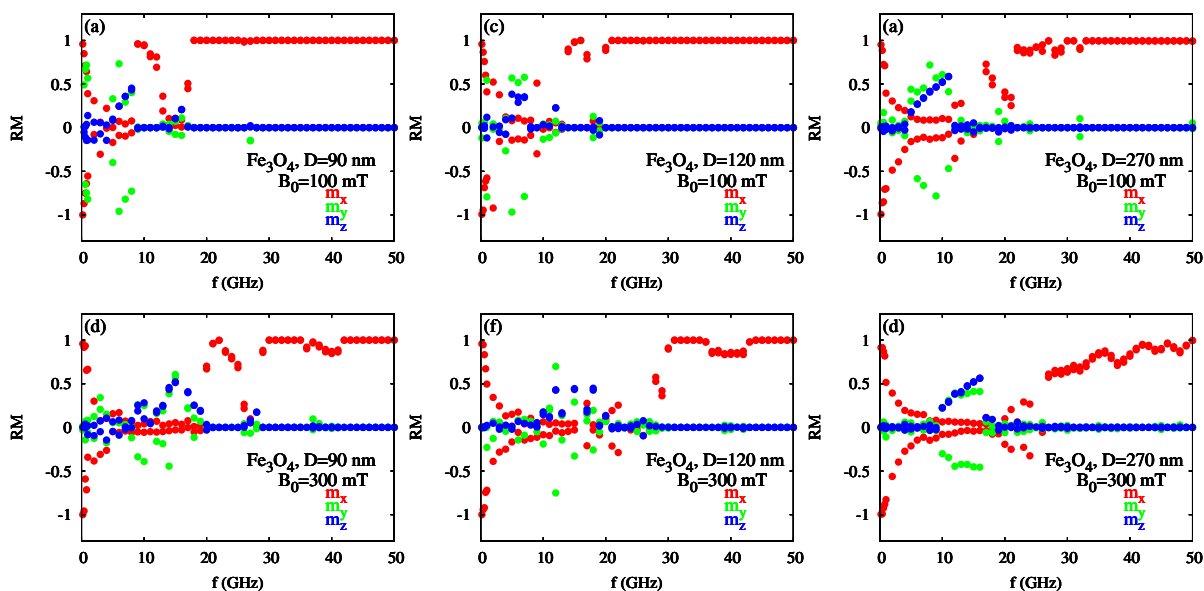


Fig. 8 Variation of RM of Fe_3O_4 as a function of frequency for different diameters and amplitudes

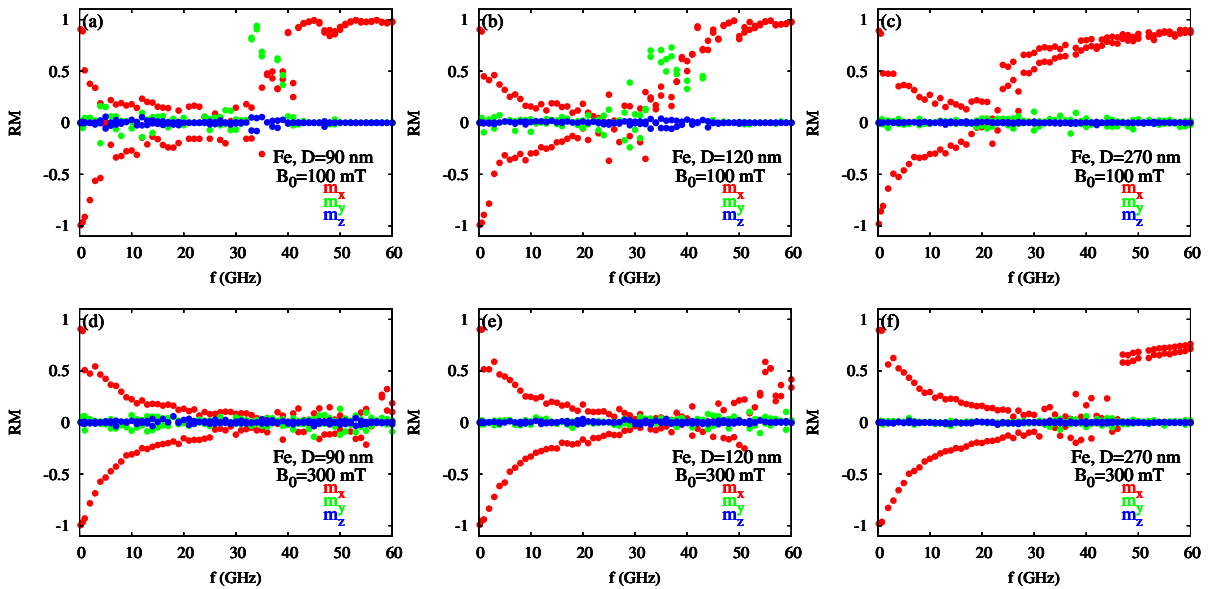


Fig. 9 Variation of RM of *Fe* as a function of frequency for different diameters and amplitudes

exhibits a transition at approximately 47 GHz. The increased amplitude made the transition to the dynamic phase more challenging at lower diameters. In contrast with *Fe₃O₄*, the system exhibits a tendency to remain in the disordered phase or dynamic paramagnetic phase.

Table 2 has been constructed to provide a more comprehensive explanation of the phase transition frequency values at which the transition from the dynamic disordered phase to the dynamic ordered phase occurs.

Lastly, we examine the dynamic hysteresis characteristic of the coercive field. The variation in CF values of *Fe₃O₄* nanodisks with frequency is displayed in Fig. 10. The CF value reflects only dynamic disordered phase behavior. In the dynamic ordered phase, the hysteresis curves do not intersect the x-axis. This signifies that no magnetic field value is necessary to alter the magnetization’s direction within the system. Consequently, as depicted in Fig. 10, there exists a CF value

for all magnetization components at low-frequency values. After these values, we can deduce that the system transitions into the dynamic ordered phase. Moreover, when the diameter increases to 270 nm in Fig. 10c and f, the formation of a neck in the CF related to the *m_x* component is clearly seen at both high and low amplitudes, without transitioning into the dynamic disordered phase within the system. This is caused by the width of the hysteresis curve increasing and decreasing again with changing frequency. With the change in frequency, not only did the phase transition occur, but also the width of the hysteresis curve varied. The irregularity of the increasing-decreasing trend at lower diameters suggests that the hysteresis undergoes constant changes with the frequency variation, indicating more frustrated behavior in the system.

In addition, the behavior we focus on as the sample diameter effect is also related to shape anisotropy. The decrease in size has also triggered an increase in the

Table 2 Estimated phase transition frequency values

<i>D</i>	<i>Fe₃O₄</i>		<i>Fe</i>	
	<i>B₀</i> = 100 mT	<i>B₀</i> = 300 mT	<i>B₀</i> = 100 mT	<i>B₀</i> = 300 mT
90 nm	9 GHz	20 GHz	35 GHz	58 GHz
120 nm	14 GHz	27 – 28 GHz	32 GHz	54 GHz
270 nm	16 GHz	27 – 28 GHz	24 GHz	47 GHz

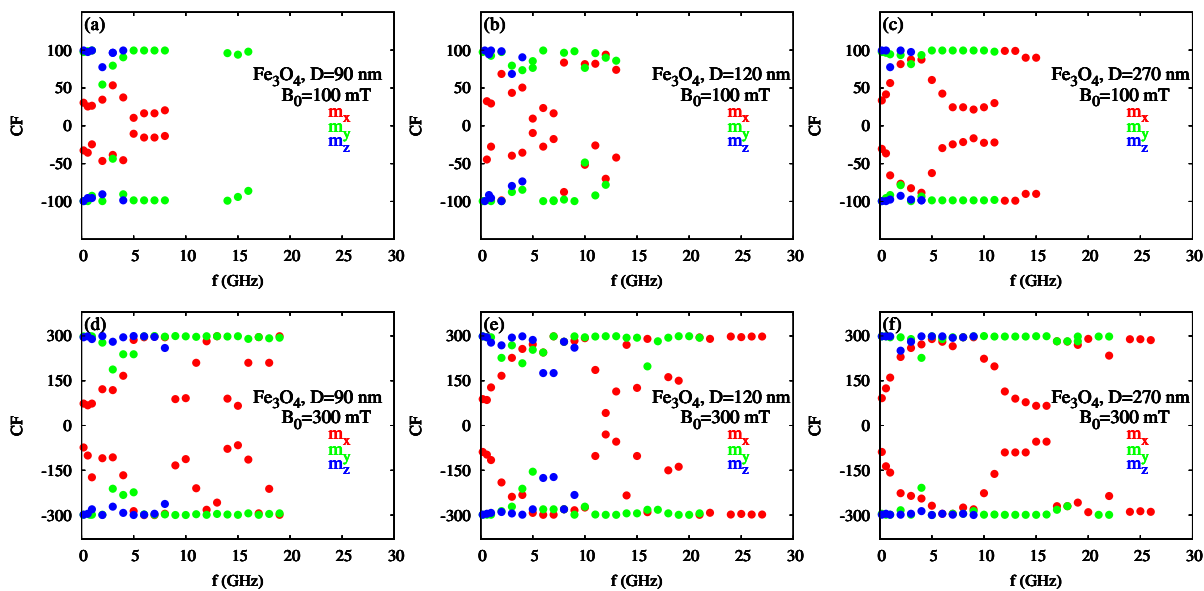


Fig. 10 Dependence of CF values of Fe_3O_4 nanodisk on changing diameter and frequency for $B_0 = 100 \text{ mT}$ $B_0 = 300 \text{ mT}$

effect of shape anisotropy. Specifically, in Fe_3O_4 nanodisks, which are characterized as soft magnetic materials compared to Fe nanodisks, the effects of shape anisotropy have caused the hysteresis loops to exhibit variations in magnetization components within the nanodisk, differing from the direction of the applied external magnetic field. This effect has become more pronounced as the diameter has decreased because most spins in a magnetic nanodisk are at the nanodisk surface where there is reduced coordination in magnetic moments. This situation also explains the frustrated behavior observed at RM values. In the Fe_3O_4 system, shape anisotropy is dominant because magneto-crystalline energy is completely ignored, resulting in more pronounced frustrated behaviors. On the other hand, in the Fe nanosystem, as the diameter increases, the effect of shape anisotropy diminishes compared to the moderate magneto-crystalline energy, leading to the disappearance of frustrated behavior, especially when $D = 270 \text{ nm}$.

Our simulation results demonstrate that as the diameter increased, the behavior of the magnetization components along the y and z directions diminished in Fe_3O_4 and disappeared in Fe nanodisk. As systems generally possess more magnetic moments with increasing diameter, the overall magnetic interaction within the system becomes stronger. The surface effect diminishes, and a more collective magnetic behavior

occurs, with the influence of magnetic moments behaving differently in various directions becoming less noticeable. The increase in the magnitude of the magnetic field also suppresses the effect of shape anisotropy triggered by the decrease in size, as it forces the magnetic moments in the system to align in the same direction as the field, thereby mitigating the different magnetization components' magnetic response.

The behavior of CF for the Fe nanodisks depending on the frequency and changing particle size is also shown in Fig. 11. In line with the HLA and RM curves, detailed observation of dynamic disordered phase behavior is noted in CF. We can observe the variation in hysteresis curve widths as the frequency changes within CF. In Fig. 11, it is observed that the CF values exhibit a noteworthy trend. As illustrated in Fig. 11, the CF values initially manifest at a minimum level corresponding to the initial frequency. Subsequently, with an increase in frequency, these values ascend to a peak before subsequently declining. While the maximum values of the CF curves show an increasing trend with higher amplitude values in Fig. 11d–f, it is noteworthy that at the initial frequency value, CF values are higher at lower amplitudes, as depicted in Fig. 11a–c. On the other hand, CF values corresponding to hysteresis formed by m_y and m_z magnetization components are observed by small diameters in Fig. 11a–e. While increasing the amplitude destroyed the magnetic

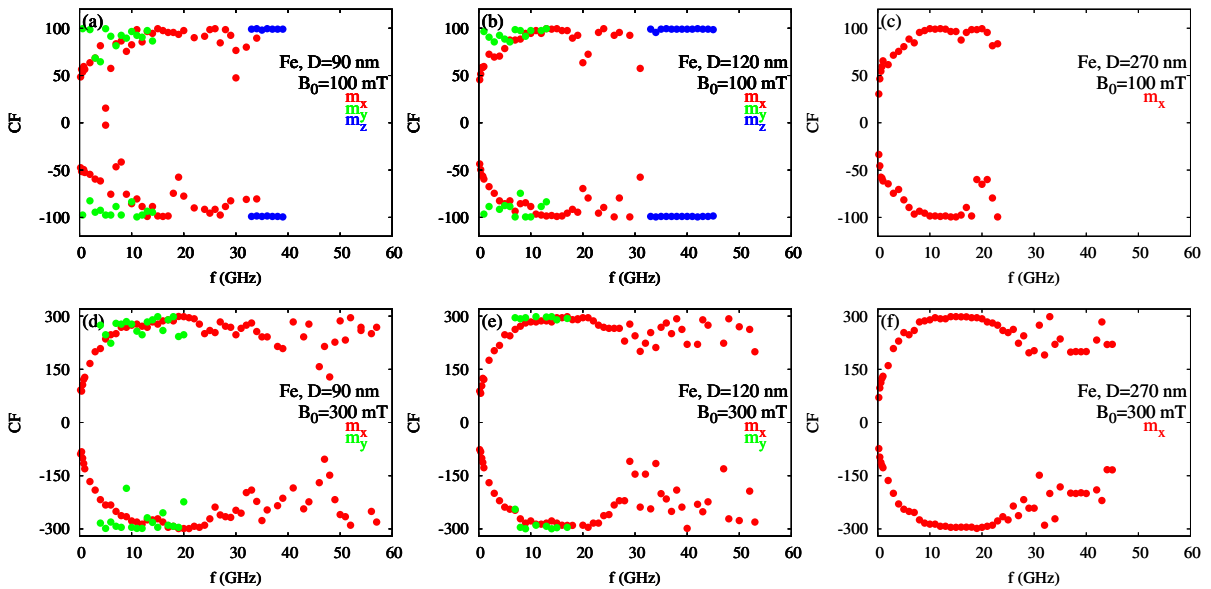


Fig. 11 Dependence of CF values of *Fe* nanodisk on changing diameter and frequency for $B_0 = 100\text{ mT}$ $B_0 = 300\text{ mT}$

behavior the m_z , increasing the diameter destroyed the magnetic behavior of m_y .

In general, when comparing RM or CF curves, it is observed that the hysteresis widths formed by the *Fe* nanodisks are greater than that of the Fe_3O_4 nanodisk.

4 Conclusion

The impact of size on the dynamic magnetic properties and dynamic phase transitions of *Fe* and Fe_3O_4 2D circular nanodisks with varying diameters has been thoroughly investigated under an externally applied dynamic magnetic field in the x-direction. This investigation has been carried out by micromagnetic simulation OOMMF software to solve the nonlinear LLG equation in detail.

Firstly, the diameter of the system plays a pivotal role in determining its dynamic magnetic properties. As the diameter decreases, the dynamic ordered phase behavior differs between *Fe* and Fe_3O_4 nanodisks. Frequency values increase for the transition to a dynamic ordered phase in *Fe* nanodisks, whereas a decrease is observed in Fe_3O_4 nanodisks. At low amplitudes and small diameter values, dynamically ordered phase behavior has been simultaneously observed in *Fe* nanodisks in both the x and y directions within a certain

frequency range. On the other hand, in the Fe_3O_4 nanodisks, dynamic order behavior emerged in the z direction before the magnetization component transitioned to the dynamically ordered phase in the x direction in different frequency ranges, while dynamically disordered phase behavior emerged in the x and y directions. Generally, increasing the diameter led to improvements in the trends of HLA, CF, and RM curves in both systems. Because the systems generally possess more magnetic moments that are related to growing diameter. The overall magnetic interaction within the system becomes stronger. This can lead to more pronounced magnetic effects.

An increase in amplitude leads to a shift towards higher frequency values, at which phase transitions are observed. At low amplitudes and diameters, *Fe* nanodisks exhibit a tendency to remain in the dynamic paramagnetic phase, contrary to Fe_3O_4 . The simulation results emphasize that increasing the frequency not only determines the occurrence of phase transitions but also influences changes in the widths of the hysteresis curves, as evident from the CF curves. Therefore, our results may contribute to the literature in terms of hyperthermia treatment and data storage devices.

Acknowledgements The author is grateful to Ümit Akıncı from Department of Physics, Dokuz Eylül University for his valuable suggestions.

Author contributions Writing original draft, visualization, investigation, formal analysis, writing—review and editing.

Data Availability Statement Data will be made available on request.

Declarations

Conflict of interest The author declares no competing interests.

References

1. De D, Goswami S, Chakraborty M (2023) Magnetic memory effect: unfolding magnetic metastabilities. *J Magn Magn Mater* 565:170175. <https://doi.org/10.1016/j.jmmm.2022.170175>
2. Rocha-Santos TA (2014) Sensors and biosensors based on magnetic nanoparticles. *TrAC, Trends Anal Chem* 62:28–36. <https://doi.org/10.1016/j.trac.2014.06.016>
3. Bañobre-López M, Teijeiro A, Rivas J (2013) Magnetic nanoparticle-based hyperthermia for cancer treatment. *Reports of Practical Oncology & Radiotherapy* 18(6):397–400. <https://doi.org/10.1016/j.rpor.2013.09.011>
4. Khan AU, Chen L, Ge G (2021) Recent development for biomedical applications of magnetic nanoparticles. *Inorg Chem Commun* 134:108995. <https://doi.org/10.1016/j.inoche.2021.108995>
5. Tang SC, Lo IM (2013) Magnetic nanoparticles: essential factors for sustainable environmental applications. *Water Res* 47(8):2613–32. <https://doi.org/10.1016/j.watres.2013.02.039>
6. Zhou K, Zhou X, Liu J, Huang Z (2020) Application of magnetic nanoparticles in petroleum industry: a review. *J Petrol Sci Eng* 188:106943. <https://doi.org/10.1016/j.petrol.2020.106943>
7. Lamouri R, Mounkachi O, Salmani E, Hamedoun M, Benyoussef A, Ez-Zahraouy H (2020) Size effect on the magnetic properties of CoFe₂O₄ nanoparticles: a Monte Carlo study. *Ceram Int* 46(6):8092–6. <https://doi.org/10.1016/j.ceramint.2019.12.035>
8. Kachkachi H, Nogues M, Tronc E, Garanin DA (2020) Finite-size versus surface effects in nanoparticles. *Journal of magnetism and magnetic materials* 221(1-2):158–63. [https://doi.org/10.1016/S0304-8853\(00\)00390-5](https://doi.org/10.1016/S0304-8853(00)00390-5)
9. Iglesias Ò, Labarta A. (2004) Influence of surface anisotropy on the magnetization reversal of nanoparticles. *physica status solidi (c)* 1(12):3481–4. <https://doi.org/10.1002/pssc.200405485>
10. Ma Z, Mohapatra J, Wei K, Liu JP, Sun S (2021) Magnetic nanoparticles: synthesis, anisotropy, and applications. *Chem Rev* 123(7):3904–43. <https://doi.org/10.1021/acs.chemrev.1c00860>
11. Mohapatra J, Joshi P, Liu JP (2023) Low-dimensional hard magnetic materials. *Prog Mater Sci* 138:101143. <https://doi.org/10.1016/j.pmatsci.2023.101143>
12. Shava B, Ayodeji FD, Rahdar A, Iqbal HM, Bilal M (2022) Magnetic nanoparticles-based systems for multifaceted biomedical applications. *Journal of Drug Delivery Science and Technology* 74:103616. <https://doi.org/10.1016/j.jddst.2022.103616>
13. Farzanegan Z, Tahmasbi M. Evaluating the applications and effectiveness of magnetic nanoparticle-based hyperthermia for cancer treatment: a systematic review (2023) *Applied Radiation and Isotopes* 198:110873. <https://doi.org/10.1016/j.apradiso.2023.110873>
14. Dantas CC, Gama AM. Micromagnetic simulations of spinel ferrite particles (2010) *Journal of magnetism and magnetic materials* 322(19):2824–33. <https://doi.org/10.1016/j.jmmm.2010.04.037>
15. Maniotis N (2023) Studying the rate-dependent specific absorption rate in magnetic hyperthermia through multiscale simulations. *AIP Advances* 13(6). <https://doi.org/10.1063/5.0147924>
16. Anand M (2021) Dipolar interaction and sample shape effects on the hysteresis properties of 2d array of magnetic nanoparticles. *Pramana* 95:1–9. <https://doi.org/10.1007/s12043-021-02222-w>
17. Nomura E, Chiba M, Matsuo S, Noda C, Kobayashi S, Manjanna J, Kawamura Y, Ohishi K, Hiroi K, Suzuki JI (2022) Magnetization process of cubic Fe₃O₄ submicron particles studied by polarized small-angle neutron scattering. *AIP Advances* 12(3). <https://doi.org/10.1063/9.0000318>
18. Haseeb M, Li YQ, Zhang HG, Liu WQ, Zhang PJ, Yue M (2024) Influence and mechanism of surface defects on coercivity of M-type ferrite particles. *Surfaces and Interfaces* 46:104153. <https://doi.org/10.1016/j.surfin.2024.104153>
19. Jalali MH, Shams MH, Gholizadeh H (2023) Micromagnetic simulation of the shape effect on the permeability and loss tangent of Fe₃O₄ nanoparticles in the microwave range. *J Supercond Novel Magn* 36(2):601–9. <https://doi.org/10.1007/s10948-022-06452-w>
20. Tsuji T, Kobayash S (2024) Enhanced heating efficiency for hollow Fe₃O₄ spherical submicron particles. *AIP Advances* 14(1). <https://doi.org/10.1063/9.0000695>
21. Anand M, Carrey J, Banerjee V (2018) Role of dipolar interactions on morphologies and tunnel magnetoresistance in assemblies of magnetic nanoparticles. *J Magn Magn Mater* 454:23–31. <https://doi.org/10.1016/j.jmmm.2018.01.027>
22. Dantas CC (2021) Analysis of the collective behavior of a 10 by 10 array of Fe₃O₄ dots in a large micromagnetic simulation. *Physica E* 44(3):675–9. <https://doi.org/10.1016/j.physe.2011.11.007>
23. Roa N, Restrepo J (2023) Micromagnetic approach to the metastability of a magnetite nanoparticle and specific loss power as function of the easy-axis orientation. *Physchem* 3(3):290–303. <https://doi.org/10.3390/physchem3030020>
24. Ehrmann A, Blachowicz T (2015) Influence of shape and dimension on magnetic anisotropies and magnetization reversal of Py, Fe, and Co nano-objects with four-fold symmetry. *AIP Advances* 5(9). <https://doi.org/10.1063/1.4930532>
25. Bachar F-Z, Schröder C, Ehrmann A (2021) Magnetization reversal in Pac-Man shaped Fe nanostructures with varying aperture. *J Magn Magn Mater* 537:168205. <https://doi.org/10.1016/j.jmmm.2021.168205>
26. Leighton B, Vargas NM, Altbir D, Escrib J (2011) Tailoring the magnetic properties of Fe asymmetric nanodots. *J Magn Magn Mater* 323(11):1563–7. <https://doi.org/10.1016/j.jmmm.2011.01.019>

27. Djuhana D, Kadir JA, Widodo AT, Kim DH (2014) Micromagnetic study on the dynamic susceptibility spectra of square-patterned ferromagnets. *Advanced Materials Research* 896:410–3. <https://doi.org/10.4028/www.scientific.net/AMR.896.410>
28. Djuhana D, Kurniawan C, Widodo AT (2019) Dynamic susceptibility spectra analysis of ferromagnetic spheres via micromagnetic simulations. In *IOP Conference Series: Materials Science and Engineering* 496:012027. <https://doi.org/10.1088/1757-899X/496/1/012027>
29. Palma JL, Morales-Concha C, Leighton B, Altbir D, Escrig J (2012) Micromagnetic simulation of Fe asymmetric nanorings. *J Magn Magn Mater* 324(4):637–41. <https://doi.org/10.1016/j.jmmm.2011.09.001>
30. Öncü E, Ehrmann A (2021) Magnetization reversal in concave iron nano-superellipses. *Condensed Matter* 6(2):17. <https://doi.org/10.3390/condmat6020017>
31. Dang Xuan N, Döpke C, Blachowicz T, Ehrmann A (2020) Magnetization reversal in hexagonal nanomagnets. *Acta Physica Polonica: A* 137(3). <https://doi.org/10.12693/APhysPolA.137.395>
32. López-Urías F, F, Torres-Heredia JJ, Muñoz-Sandoval (2005) Magnetization patterns simulations of Fe, Ni Co, and permalloy individual nanomagnets. *J Magn Magn Mater* 294(2):e7-12. <https://doi.org/10.1016/j.jmmm.2005.03.044>
33. Donahue MJ, Porter DG (1999) NISTIR No. 6376
34. Trudel S, Gaier O, Hamrle J, Hillebrands B (2010) Magnetic anisotropy, exchange and damping in cobalt-based full-Heusler compounds: an experimental review. *J Phys D Appl Phys* 43(19):193001. <https://doi.org/10.1088/0022-3727/43/19/193001>
35. Kronmüller H (2003) *Micromagnetism and the microstructure of ferromagnetic solids*. Cambridge University Press
36. Saavedra E, Corona RM, Vidal-Silva N, Palma JL, Altbir D, Escrig J (2020) Dynamic and static properties of stadium-shaped antidot arrays. *Scientific Reports* 10(1):20024. – <https://doi.org/10.1038/s41598-020-77074-2>

Publisher's Note Springer Nature remains neutral with regard to jurisdictional claims in published maps and institutional affiliations.

Springer Nature or its licensor (e.g. a society or other partner) holds exclusive rights to this article under a publishing agreement with the author(s) or other rightsholder(s); author self-archiving of the accepted manuscript version of this article is solely governed by the terms of such publishing agreement and applicable law.